

Spin Hall effect and Zitterbewegung in an electron waveguide

P. Brusheim* and H. Q. Xu†

Division of Solid State Physics, Lund University, Box 118, S-22100 Lund, Sweden.

(Dated: June 24, 2018)

We study spin-resolved probability distributions for electrons in a multi-channel waveguide in the presence of spin-orbit interaction. For a spin-polarized electron injection, a Zitterbewegung pattern is predicted in the probability distribution of the electrons in the waveguide. For a spin-unpolarized injection, the spin-resolved electron probability in the waveguide shows spin accumulations. In addition to the spin Hall phenomenon, namely accumulations of opposite spins at the lateral edges of the waveguide, we predict the existence of a regular stripe pattern of spin accumulations in the internal region of the waveguide. We show that the predicted Zitterbewegung and spin Hall effect stem from the same mechanism and are formed from coherent states of electrons in the waveguide.

PACS numbers: 72.25.Dc, 71.70.Ej, 85.75.Nn, 73.23.Ad

Spin-orbit interaction (SOI) is a relativistic effect: it arises from the fact that an electron moving with a finite momentum in a non-uniform electric potential will see an effective magnetic field acting on its spin. The SOI plays an important role in the field of spintronics since it is in most cases responsible for spin rotation and relaxation. Recently an increased interest has been focused on a consequence of the SOI, namely a spatial spin accumulation in a two-dimensional system in the absence of a magnetic field, known as the spin Hall effect.^{1,2,3,4,5,6,7,8,9,10,11,12,13,14,15,16,17} Another SOI-induced phenomenon of current interest is the *Zitterbewegung* of electrons in semiconductors,^{18,19,20} in analogy with the oscillating behavior of a free relativistic electron due to interference between its positive- and negative-energy state components. The previous theoretical studies were focused on two-dimensional systems or quasi-one-dimensional systems with electron injection in the lowest subband only. However, in a realistic experimental setup the Fermi energy and width of the sample are often set at values for which the electron transport is in the multi-subband (multi-channel) regime. It is known that the SOI will induce interaction between subbands as well as the spin states.^{21,22,23} These interactions will bring an initially prepared spin state into a quantum-coherent spin-mixed state and can give rise to complicated spin-dependent electron transport phenomena. To capture all the physics of the problem an exact multi-subband treatment is hence necessary.

It has been theoretically shown that the vertex corrections will cancel the transverse spin current in an infinite system.^{12,13,14,15,16} However, the disappearance of a transverse spin current does not exclude the existence of spatial spin density modulations arising as a coherent interference effect. Reynoso, Usaj and Balseiro have recently studied the spin Hall effect as a coherent phenomena in a finite system by calculating the expectation value of the spin operators.¹⁷ In this paper we will calculate the wavefunction and its individual spin components to study the intrinsic spin-Hall effect and Zitterbewegung in a multi-channel electron waveguide in the absence of an external magnetic field. We will show that the Zitter-

bewegung and the intrinsic spin Hall effect is essentially the same kind of phenomena. We will further show the existence of a reversal of the direction of spatially accumulated spins for electrons injected from individual channels in the waveguide, which can not be explained by a simple heuristic force operator consideration previously adopted in the literature. We will also show that regular stripe patterns of spin accumulations are formed inside the multi-channel waveguide in addition to the usual edge spin accumulations found in the spin Hall effect. These patterns are shown to arise from coherent states in the waveguide and the number of stripes in the patterns are found to be related to the number of open channels in the leads.

To study the problem we consider a two-dimensional electron gas (2DEG) formed in the x - y plane of a semiconductor heterostructure. The 2DEG is restricted to a waveguide of width w by a hard-wall confinement potential $U_c(y)$, i.e., $U_c(y) = 0$ for $y \in [-w/2, w/2]$ and ∞ otherwise, in the transverse y -direction. The structure is subjected to an electrical field along the unit vector ξ giving rise to a Rashba SOI of strength α . For crystal structures without inversion symmetry, there will in addition be a Dresselhaus SOI contribution, characterized by the strength β . Such inversion asymmetry is found in, e.g., zinc-blende crystals of III-V materials. The waveguide is connected with two perfect leads with vanishing SOI. The electrons are injected from one of the two leads into the region with a finite SOI and transport coherently in the longitudinal x -direction. The model Hamiltonian describing such a system under the effective mass approximation has the form,

$$H = \sigma_0 \left[\frac{\mathbf{p}^2}{2m^*} + U_c(y) \right] + \frac{1}{2\hbar} \left[\alpha(\mathbf{r}) \boldsymbol{\sigma} \cdot (\mathbf{p} \times \boldsymbol{\xi}) + \beta(\mathbf{r}) (\sigma_x p_x - \sigma_y p_y) + H.c. \right], \quad (1)$$

where \mathbf{p} is the momentum operator, m^* the electron effective mass, which is taken to be $m^* = 0.042 m_e$ corresponding to an InGaAs quantum-well system, $\boldsymbol{\sigma} = (\sigma_x, \sigma_y, \sigma_z)$ the vector of the Pauli matrices, and σ_0 the unit matrix. The inclusion of the SOI breaks the reflec-

tion invariance of the system in the transverse direction, i.e., $[R_y, H] \neq 0$. However, for a symmetric confining potential the system is invariant under operation of $\sigma_y R_y$, i.e., $[\sigma_y R_y, H] = 0$. This symmetry has an important implication: for a spin-unpolarized electron injection, the spin-up electron probability distribution in the system is exactly the mirror image of the spin-down electron probability distribution with respect to the transverse reflection R_y . Thus, if an accumulation of spin occurs on one side of the waveguide, the same amount of accumulation of the opposite spin will occur on the other side of the waveguide. Since an unpolarized electron injection beam is an incoherent mixture of two spin injections, this symmetry asserts that all information about the probability distribution, regardless of the injection condition, is contained in the probability distribution of a polarized injection beam. One needs only to consider the calculations for one spin injection, since the results from the other spin injection follows from the symmetry requirement.

The (spin-unpolarized) probability distribution, $\rho^\gamma(x, y)$, for electrons injected from a lead in a spin- γ state can be obtained from

$$\rho^\gamma(x, y) = \sum_{q\sigma} \rho_q^{\sigma\gamma}(x, y) \sim \sum_{\sigma} \sum_{\{q|k_q \in \mathbb{R}\}} \frac{|\langle \chi(\sigma) | \Psi_q^\gamma(x, y) \rangle|^2}{k_q}, \quad (2)$$

where $\Psi_q^\gamma(x, y)$ is the wave function of an electron injected from the lead in the q th subband with spin $\gamma = \uparrow$ or \downarrow , $|\chi(\gamma = \uparrow)\rangle = (1, 0)^T$ and $|\chi(\gamma = \downarrow)\rangle = (0, 1)^T$ are the two spin states with the spin quantization axis along the electric field direction, $k_q = [2m^*(E_F - E_q)/\hbar^2]^{1/2}$ with E_F being the Fermi energy and E_q the q th subband energy in the injection lead, and $\rho^{\sigma\gamma}(x, y)$ is the spin- σ probability distribution. In the present work, the wave function Ψ_q^γ has been calculated by employing an exact, spin-dependent, multi-mode scattering matrix technique (see Refs. 23,24,25 for the detail of the theoretical method).

Consider now the case when only the Rashba SOI is present, i.e., $\beta = 0$ and $\alpha \neq 0$, in Eq. (1). Since $[\sigma_i, H] \neq 0$ for all i , an electron initially prepared in a pure spin state in the lead will evolve into a quantum-coherently spin-mixed state as it travels in the waveguide with a finite SOI. This coherent spin evolution will give rise to a spin density modulation along the waveguide. To visualize these properties, we calculate the electron probability distributions in the waveguide. We consider the common situation with the electric field, ξ , set along the z -direction. In this case, the Rashba SOI term can be written as $(\alpha/2\hbar)(\sigma_x p_y - \sigma_y p_x) + H.c.$

We first assume the width of the waveguide $w = 100$ nm and the Fermi energy $E_F = 2$ meV, corresponding to the case where only one channel is open in the leads. The SOI strength is taken to be $\alpha = 3 \times 10^{-11}$ eVm in the region with the full strength of the Rashba SOI, defined in $x \in [0, 800]$ nm, and decreased adiabatically down to zero in the transition regions of the entrance and exit, defined in $x \in [-100, 0]$ and $x \in [800, 900]$ nm, respec-

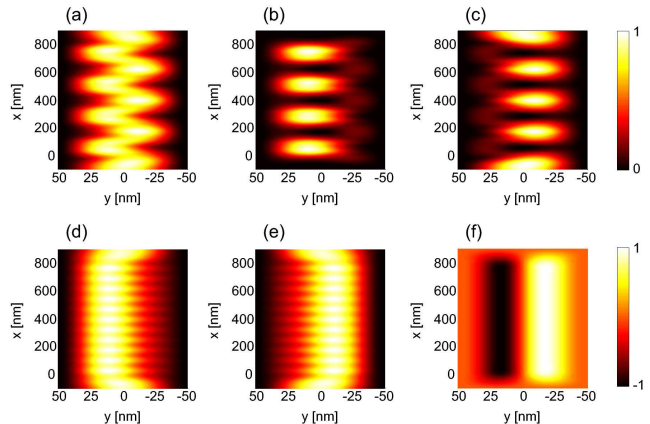


FIG. 1: (Color online) Normalized probability distribution for electrons injected in a spin-up state (a)-(b) and for a spin-unpolarized electron injection (d)-(f). (a) is for probability distribution, ρ_1^\uparrow ; (b) for its spin-down projection, $\rho_1^{\downarrow\uparrow}$; (c) for its spin-up projection, $\rho_1^{\uparrow\downarrow}$; (d) for the probability distribution of spin-down electrons in the spin-unpolarized injection, $\rho_1^{\downarrow\uparrow} + \rho_1^{\downarrow\downarrow}$; (e) for the probability distribution of spin-up electrons in the spin-unpolarized injection, $\rho_1^{\uparrow\uparrow} + \rho_1^{\uparrow\downarrow}$; and (f) for the spin polarization distribution in the spin-unpolarized electron injection, $\rho_{1,pol} = \rho_1^{\uparrow\uparrow} + \rho_1^{\uparrow\downarrow} - \rho_1^{\downarrow\uparrow} - \rho_1^{\downarrow\downarrow}$. In all the figures, the channel width is set at $w = 100$ nm and the Rashba SOI strength is $\alpha = 3 \times 10^{-11}$ eVm for $x \in [0, 800]$ nm and is decreased adiabatically down to zero in $x \in [-100, 0] \cup [800, 900]$ nm. The Fermi energy is set at $E_F = 2$ meV. The upper scale bar shows the measure for plots (a)-(e), while the lower scale bar shows the measure for plot (f).

tively. Figure 1(a) shows the calculated total (charge) probability distribution $\rho^\uparrow = \rho^{\uparrow\uparrow} + \rho^{\downarrow\uparrow}$ for electrons injected in a pure spin-up state from the lower lead. It is seen that the electron wave function exhibits a transversely oscillating behavior along the waveguide. This is the Zitterbewegung arising from interference between the two spin components of the electron state. By considering the spin-up [Fig 1(b)] and the spin-down [Fig 1(c)] projections separately, spin-wave patterns, in the form of spatially separated localized islands of high spin distribution density, are found. The two probability distribution components, $\rho^{\uparrow\downarrow}$ and $\rho^{\downarrow\downarrow}$, for the spin-down injection can be obtained from mirror reflection of the results shown in Figs. 1(a)–1(c) as required by $[\sigma_y R_y, H] = 0$. It is evident that the spin-up and spin-down electron wave-function components are localized in different sides of the waveguide. This accumulation of different spins along opposite edges of the waveguide is a fundamental property of the spin Hall effect observed recently. The spin projected electron probability distributions for a spin-unpolarized injection are shown in Figs. 1(d) and 1(e). Due to the symmetry of the system under the operation of $\sigma_y R_y$, the total distribution will be symmetrical in the transverse direction, and the spin-up (spin-down) probability distribution, Fig. 1(d) [Fig. 1(e)], is the mirror image of

the corresponding spin-down (spin-up) probability distribution. Hence no spin-polarization will be detected in the measured two-terminal conductance. This was rigorously shown, in Refs. 26 and 27, to be always hold, independent of the details of the conductor, when only one channel is open for conduction in the leads. Accumulations of electron spins with opposite polarizations at the opposite edges of a wide conductor have recently been experimentally observed^{6,7,8}. What is measured in such experiments is the net spin density distribution, $\rho_{pol} = \rho^{\uparrow\uparrow} + \rho^{\uparrow\downarrow} - \rho^{\downarrow\uparrow} - \rho^{\downarrow\downarrow}$, in the sample for a spin-unpolarized electron injection. Figure 1(f) displays the results of calculations for ρ_{pol} in the waveguide and shows clearly the signature of the spin Hall effect. It is seen that the spin Hall effect and the Zitterbewegung is essentially the same kind of phenomena, since one follows from the other, depending on if only one or both spin states are considered in the injection source and whether the spin accumulation or the charge accumulation is measured. In other words, the results of Figs. 1(a), 1(d), 1(e) and 1(f) can be constructed from Figs. 1(b) and 1(c) and their mirror images.

When the Fermi energy is increased, more channels are open for conduction in the leads. Figure 2 shows the probability distributions for the Fermi energy set at $E_F = 12$ meV, for which three spin-degenerate channels are open for conduction in the leads. In Figs. 2(a)-2(f), the spin probability distributions for spin-up electrons injected from the lower lead in the three individual channels are shown. The probability distributions for the spin-up injection in the lowest channel, $\rho_1^{\uparrow\uparrow}$ and $\rho_1^{\uparrow\downarrow}$, shown in Figs. 2(a) and 2(b) exhibit similar Zitterbewegung and spin-Hall patterns as was found in the single-channel system. However, here a reversal of the spin-polarization direction is found: the spin-up (spin-down) probability density is localized along the left (right) edge of the waveguide. This is also true for the probability distributions for the spin-up injection in the second lowest channel, $\rho_2^{\uparrow\uparrow}$ and $\rho_2^{\uparrow\downarrow}$, as shown in Figs. 2(c) and 2(d). Only the probability distributions for the spin-up injection in the highest subband, $\rho_3^{\uparrow\uparrow}$ and $\rho_3^{\uparrow\downarrow}$, shown in Figs. 2(e) and (f), exhibit the same spin parity as in the single-channel opening case. We note that this phenomenon can not be explained by the force operator, derived from the Hamiltonian, as in, e.g., Ref 10, and implies that such a heuristic approach fails to explain the full quantum mechanical calculations. Indeed, for equilibrium systems considered here, no physical force is present and the observed Zitterbewegung and spin-Hall effect are non-dynamical but merely coherent phenomena.

In light of these findings, one may ask if the Zitterbewegung and spin-Hall effect can still be observed in the multi-channel system when the contributions from all the individual channel injections are taken into account. To answer this question we show the total probability distribution, ρ^\uparrow , for a spin-up electron injection in the waveguide in Fig. 2(g) and the spin polarization distribution, ρ_{pol} , for a spin-unpolarized electron injection in Fig. 2(h).

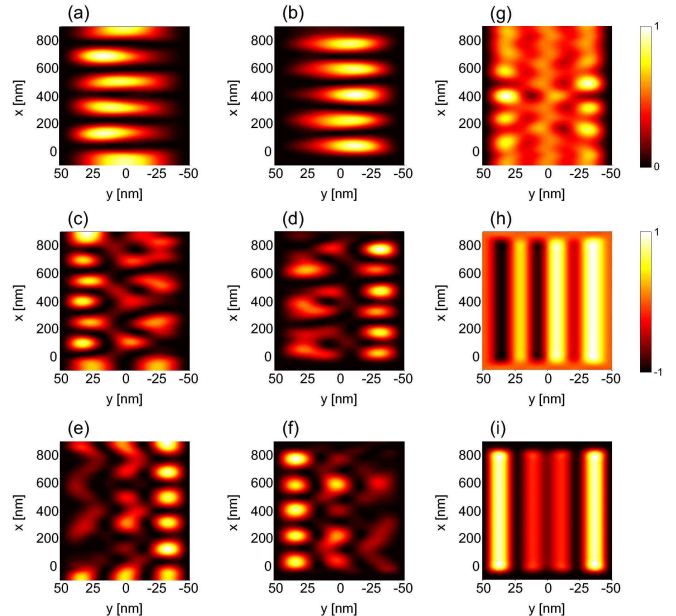


FIG. 2: (Color online) Normalized electron probability distribution and spin-projected electron probability distribution for spin-polarized and spin-unpolarized injections in the same waveguide as in Fig. 1 at the Fermi energy $E_F = 12$ meV (the case with three opening channels in the leads). (a) is for $\rho_1^{\uparrow\uparrow}$; (b) for $\rho_1^{\uparrow\downarrow}$; (c) for $\rho_2^{\uparrow\uparrow}$; (d) for $\rho_2^{\uparrow\downarrow}$; (e) for $\rho_3^{\uparrow\uparrow}$; (f) for $\rho_3^{\uparrow\downarrow}$; (g) is the the normalized total probability distribution for spin-up electron injection, $\rho^\uparrow = \sum_{q=1}^3 (\rho_q^{\uparrow\uparrow} + \rho_q^{\downarrow\uparrow})$; (h) is the normalized total spin distribution for spin-unpolarized electron injection, $\rho_{pol} = \sum_{q=1}^3 (\rho_q^{\uparrow\uparrow} + \rho_q^{\downarrow\downarrow} - \rho_q^{\uparrow\downarrow} - \rho_q^{\downarrow\uparrow})$; and (i) the same as (h) but for the distribution of the spin polarization along the transverse y direction. The upper scale bar shows the measure for plots (a)–(g) and (i), while the lower scale bar shows the measure for plot (h).

It is seen in Fig. 2(g) that Zitterbewegung oscillations are still found along the waveguide, albeit more complicated as compared to the single-channel opening case. The spin polarization distribution, ρ_{pol} , shown in Fig. 2(h) exhibits a regular spin density pattern. Strong spin polarization with opposite sign is found at the two edges of the waveguide, as observed in recent experiments. However, spin accumulation, with a pattern of alternative spin-polarization stripes, also occurs inside the waveguide. The number of stripes (including the edge spin polarization stripe) for each spin-polarization direction is equal to the number of the open channels in the waveguide. Experimental observation of the interesting internal spin-polarization structure is certainly challenging; it requires a spin detection setup with a high spatial resolution (about 50 nm or better for the system discussed in this work). However, it should be noted that no spin Hall effect could be observed if the spin polarization along a direction perpendicular to the electric field z direction is measured in the system. Although the spin polarization along the transverse y direction shows a regular stripe

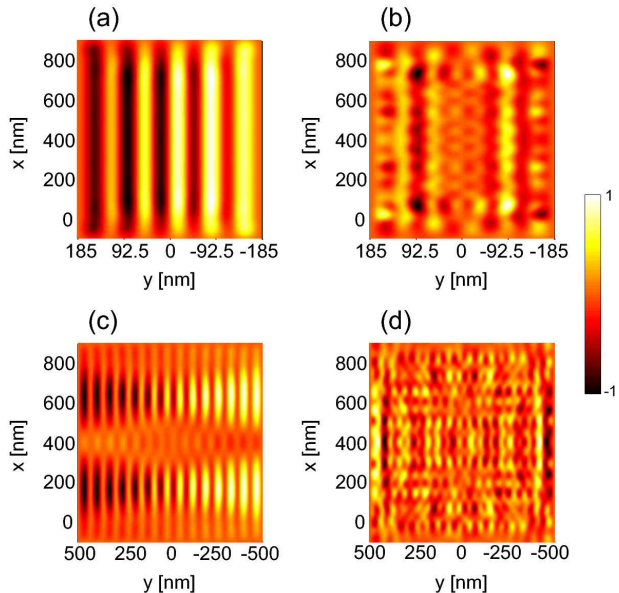


FIG. 3: (Color online) Normalized spin probability distribution, ρ_{pol} , for spin-unpolarized electron injection at the Fermi energy $E_F = 2$ meV in a waveguide with (a) $w = 370$ nm and $\alpha = 1 \times 10^{-11}$ eVm, (b) $w = 370$ nm and $\alpha = 3 \times 10^{-11}$ eVm, (c) $w = 1000$ nm and $\alpha = 0.1 \times 10^{-11}$ eVm, and (d) $w = 1000$ nm and $\alpha = 3 \times 10^{-11}$. The other waveguide parameters assumed are the same as in Figs. 1 and 2.

pattern of accumulation, the same spin polarity is seen in all the stripes, as is shown in Fig. 2(i). This can be understood as a result of polarization (or magnetization) by the effective transverse magnetic field arising from the Rashba term.

For a wide conductor, a large number of channels are typically open for conduction and the inter-subband mixing induced by the SOI can produce a complicated pattern in the electron probability distribution. In Fig. 3 we show the calculated spin polarization ρ_{pol} for a spin-unpolarized electron injection at the Fermi energy $E_F = 2$ meV in a waveguide of width $w = 370$ nm (with five open channels) and a waveguide of width $w = 1 \mu\text{m}$ (with 14 open channels) at weak and strong SOI strengths. The distributions are symmetric with respect to $\sigma_y R_y$. For the weak SOI strength, the same structural patterns of alternative spin-polarization stripes [Figs 3(a) and 3(c)] as observed in the narrower waveguide are found. For the

strong SOI strength, the spin-polarization distribution patterns [Figs. 3(b) and 3(d)] show complex structures. Although spatial spin accumulations are observable even under these circumstances, regular spin accumulations at the edges of the waveguides and internal stripe structures are destroyed by the strong SOI induced inter-channel scattering. This result indicates that the regular spin Hall effect can only be clearly observed in a range of SOI strengths in a wide, multi-channel electron waveguide.

Since the Rashba and the Dresselhaus term in the Hamiltonian are related through a unitary transformation, with the substitutions of $\sigma_x \rightarrow \sigma_y$, $\sigma_y \rightarrow \sigma_x$ and $z \rightarrow -z$, the fundamental results presented above hold for the case of $\alpha = 0$ and $\beta \neq 0$, i.e., when only the Dresselhaus SOI is present. For $\alpha = \pm\beta$ the spin-dependent part of the Hamiltonian takes the form

$$H_{\pm}^s = \frac{\alpha}{\hbar} (p_y \pm p_x) \boldsymbol{\sigma} \cdot (\mathbf{e}_x \mp \mathbf{e}_y). \quad (3)$$

The SOI induced effective magnetic field direction is in this case independent of the momentum. This means that a well-defined spin quantization axis can be found throughout the SOI region and spin is therefore a conserved quantity. In Ref. 28, it was shown that in III-V systems the Rashba and Dresselhaus SOIs can be of comparable strengths. This would imply that no Zitterbewegung¹⁸ nor spin-Hall effect could occur in this situation.

In conclusion, we have studied the total and spin-resolved electron probability distributions in a ballistic waveguide with SOI. For a spin-polarized electron injection, a Zitterbewegung pattern is observed in the probability distribution of the electrons in the waveguide. For a spin-unpolarized injection, the spin-resolved electron probability in the waveguide shows spin accumulations. The intrinsic spin Hall effect, namely accumulations of opposite spins at the lateral edges of the waveguide, can be observed in the SOI region. We have also predicted the existence of a regular stripe pattern of spin accumulations inside the waveguide. Finally we have shown that the Zitterbewegung and the spin Hall effect found in this work stem from the same mechanism and are formed from the coherent states of electrons in the waveguide.

This work was supported by the Swedish Research Council (VR) and by the Swedish Foundation for Strategic Research (SSF) through the Nanometer Structure Consortium at Lund University.

* Electronic address: Patrik.Brusheim@ftf.lth.se

† Corresponding author; Electronic address: Hongqi.Xu@ftf.lth.se

¹ J. E. Hirsch, Phys. Rev. Lett. **83**, 1834 (1999).

² S. Zhang, Phys. Rev. Lett. **85**, 393 (2000).

³ L. Sheng, D. N. Sheng, and C. S. Ting, Phys. Rev. Lett. **94**, 016602 (2005).

⁴ E. M. Hankiewicz, L. W. Molenkamp, T. Jungwirth, and J. Sinova, Phys. Rev. B **70**, 241301(R) (2004).

⁵ M. I. D'yakonov and V. I. Perel, JETP Lett. **13**, 467 (1971).

⁶ Y. K. Kato, R.C. Myers, A. C. Gossard, and D. D. Awschalom, Science **306**, 1910 (2004).

⁷ V. Sih, R. C. Myers, Y. K. Kato, W. H. Lau, A. C. Gossard,

- and D. D. Awschalom, *Nature Phys.* **1**, 31 (2005).
- ⁸ J. Wunderlich, B. Kaestner, J. Sinova, and T. Jungwirth, *Phys. Rev. Lett.* **94**, 047204 (2005).
- ⁹ B. K. Nikolić, S. Souma, L. P. Zárbo, and J. Sinova, *Phys. Rev. Lett.* **95**, 046601 (2005); B. K. Nikolić, L. P. Zárbo, and S. Souma, *Phys. Rev. B* **72**, 075361 (2005)
- ¹⁰ B. K. Nikolić, L. P. Zárbo, and S. Welack, *Phys. Rev. B* **72**, 075335 (2005).
- ¹¹ J. Sinova, D. Culcer, Q. Niu, N. A. Sinitsyn, T. Jungwirth, and A. H. MacDonald, *Phys. Rev. Lett.* **92**, 126603 (2004).
- ¹² E. G. Mishchenko, A. V. Shytov, and B. I. Halperin, *Phys. Rev. Lett.* **93**, 226602 (2004).
- ¹³ E. I. Rashba, *Phys. Rev. B* **70**, 201309(R) (2004).
- ¹⁴ J.-I. Inoue, G. E. W. Bauer, and L. W. Molenkamp, *Phys. Rev. B* **70**, 041303(R) (2004).
- ¹⁵ O. Chalaev and D. Loss, *Phys. Rev. B* **71**, 245318 (2005).
- ¹⁶ A. Khaetskii, *Phys. Rev. Lett.* **96**, 056602 (2006)
- ¹⁷ A. Reynoso, G. Usaj, and C. A. Balseiro, *Phys. Rev. B* **73**, 115342 (2006); G. Usaj and C. A. Balseiro, *Europhys. Lett.* **72**, 631 (2005).
- ¹⁸ J. Schliemann, D. Loss, and R. M. Westervelt, *Phys. Rev. Lett.* **94**, 206801 (2005); *ibid.*, cond-mat/0512148.
- ¹⁹ M. Lee and C. Bruder, *Phys. Rev. B* **72**, 045353 (2005).
- ²⁰ Z. F. Jiang, R. D. Li, S-C. Zhang, and W. M. Liu, *Phys. Rev. B* **72**, 045201 (2005).
- ²¹ F. Mireles and G. Kirczenow, *Phys. Rev. B* **64**, 024426 (2001).
- ²² X. F. Wang, *Phys. Rev. B* **69**, 035302 (2004).
- ²³ Lebo Zhang, P. Brusheim, and H. Q. Xu, *Phys. Rev. B* **72**, 045347 (2005).
- ²⁴ H. Q. Xu, *Phys. Rev. B* **50**, 8469 (1994); *ibid.* **52** 5803 (1995).
- ²⁵ David Yuk Kei Ko and J. C. Inkson, *Phys. Rev. B* **38**, 9945 (1988).
- ²⁶ F. Zhai and H. Q. Xu, *Phys. Rev. Lett.* **94**, 246601 (2005).
- ²⁷ E. N. Bulgakov and A. F. Sadreev, *Phys. Rev. B* **66**, 075331 (2002).
- ²⁸ J. B. Miller, D. M. Zumbühl, C. M. Marcus, Y. B. Lyanda-Geller, D. Goldhaber-Gordon, K. Campman, and A. C. Gossard, *Phys. Rev. Lett.* **90**, 076807 (2003).